Nonlinear Schrödinger equation for integrated photonics

KEVIN BACH GRAVESEN[1,2,*] ASGER BRIMNES GARDNER[1,2] EMIL ZANCHETTA ULSIG[1,2], ERIC J. STANTON[3,4,5], MIKKEL TORRILD HANSEN[1], SIMON THORNDAHL THOMSEN[1], LUCAS AHLER[1], AND NICOLAS VOLET[1,2]

[1] *Department of Electrical and Computer Engineering, Aarhus University, Aarhus, Denmark*
[2] *UVL A/S, Aarhus, Denmark*
[3] *EMode Photonix, Boulder, CO, USA*
[4] *Associate of the National Institute of Standards and Technology, Boulder, Colorado, USA*
[5] *Department of Physics, University of Colorado, Boulder, Colorado, USA*
*kbg@post.au.dk

Abstract: The foundations of nonlinear optics are revisited, and the formalism is applied to waveguide modes. The effect of loss and dispersion are included rigorously along with the vectorial nature of the modes, and a new version of nonlinear Schrödinger (NLS) equation is derived. This leads to more general expressions for the group index, for the group-index dispersion (GVD), and for the Kerr coefficient. These quantities are essential for the design of waveguides suitable for e.g. the generation of optical frequency combs and all-optical switches. Examples are given using the silicon nitride material platform. Specifically, values are extracted for the coefficients of the chi-3 tensor based on measurements of Kerr coefficients and mode simulations.

1. Introduction

The nonlinear Schrödinger (NLS) equation has been a fundamental tool in photonics for decades [1], offering insights into dispersion and the behavior of light in nonlinear optical media. Its applications, spanning optical communications [2], frequency metrology [3], spectroscopy [4], ultrafast science [5], and quantum optics [6, 7], underscore its paramount importance in modern optics. Today, the NLS equation is indispensable for modeling devices like all-optical switches [8, 9] and optical parametric oscillation (OPO) [10, 11]. These advancements in nonlinear optics have not only revolutionized chip-scale photonic capabilities but have also paved the path for breakthroughs in frequency synthesis [12], precision timing for positioning and navigation [13], frequency conversion of mid-infrared [14] to deep-UV [15] and a myriad of spectroscopic techniques [16].

Using the NLS equation, one can simulate how dispersion and nonlinearities affect the shape of an optical pulse as it propagates in a nonlinear medium [17]. The typical formalism to derive the NLS equation, inherited from bulk optics, makes simplifying assumptions such as lossless system and purely transverse fields [18, 19]. However, for a guided mode in a material with loss, these assumptions may not necessarily be valid [20].

The NLS equation is derived from first principles in the special case of degenerate four-wave mixing [21]. The presented model avoids assumptions about polarization and the plane-wave approximation while accommodating discontinuities in the permittivity. This makes it universally applicable to all waveguides, especially well-suited for heterogeneous structures [22–24]. In addition, the NLS equation is typically derived assuming the existence of the optical Kerr effect [25], whereas in this work the effect follows directly from the NLS equation. The bright soliton solution of the NLS equation is presented, from which a more general expression for the group index is found, which depends on both the dispersion and the mode field patterns. The presented derivation of the Kerr effect differs from existing literature in that the nonlinear

phase shift is proportional to the optical power instead of the intensity. This is a more relevant and convenient quantity in integrated photonics, since the optical intensity in waveguides varies significantly over the cross-section. The presented model leads to a compact expression for the Kerr coefficient given by the third-order nonlinear tensor and the mode profile. As the waveguide modes are readily simulated in available software, the presented formalism is a powerful tool for optical engineers to better design generated nonlinear phase shifts. To provide verification and an example of how this formalism can be used, examples are provided with silicon nitride Si_3N_4 based on previous studies.

2. Chief equation and NLS equation

The complex wavenumber is expressed as:

$$k = \beta + i\alpha/2 = n\omega/c \ , \tag{1}$$

where β is the wavenumber, α the attenuation coefficient, n is the effective refractive index of the relevant mode at the carrier frequency $\omega/(2\pi)$, and c is the speed of light in vacuum.

The complex electric field is decomposed as [26]:

$$\vec{\mathcal{E}} = e^{i\varphi}\mathcal{A}\,(z,t)\,\vec{\mathfrak{e}}\,(x,y)\,, \tag{2}$$

where $\varphi = kz - \omega t$. The complex vector $\vec{\mathfrak{e}}$ is the electric mode profile, which is independent of the longitudinal $\hat{z}$-direction. The complex function $\mathcal{A}$ is unitless and accounts for coupling between modes, as well as additional time dependence. This can be modeled through Fourier decomposition at different Fourier frequencies $\Omega/2\pi$. The modes are normalized with the following parameter [27]:

$$N \equiv \frac{1}{2}\iint_{\mathbb{R}^2}\left(\vec{\mathfrak{e}}\times\vec{\mathfrak{h}}^*\right)\cdot\hat{z}\,\mathrm{d}x\,\mathrm{d}y\,, \tag{3}$$

where $\vec{\mathfrak{h}}$ is the magnetic mode profile and the integration extends over the transverse plane of the waveguide. The mode profiles and the effective index are found by solving the dispersion relation [28]. The $\mathcal{A}$ function is then found by solving the chief equation, which is introduced now. It involves the following quantity:

$$K(\Omega) \equiv \frac{1}{4\mu_0\omega N}\iint_{\mathbb{R}^2}\gamma^2(\Omega)\ \vec{\mathfrak{e}}\cdot\vec{\mathfrak{e}}^*\,\mathrm{d}x\,\mathrm{d}y\,, \tag{4}$$

where μ_0 is the vacuum permeability, and the gamma factor γ is related to the material refractive index n_{mat} via:

$$\gamma(\Omega) = \Omega\, n_{\mathrm{mat}}(\Omega)/c \ . \tag{5}$$

The K parameter can be Taylor expanded around ω:

$$K(\Omega) \approx K(\omega) + (\Omega-\omega)k_1 + \sum_{m=2}^{\infty}\frac{(\Omega-\omega)^m}{m!}k_m, \tag{6}$$

with:

$$k_1 \equiv \left.\frac{\mathrm{d}K}{\mathrm{d}\Omega}\right|_{\omega}, \quad k_m \equiv \left.\frac{\mathrm{d}^m K}{\mathrm{d}\Omega^m}\right|_{\omega}. \tag{7}$$

In the presence of dispersion, nonlinearity, and a finite value of attenuation, the $\mathcal{A}$ function is found by solving:

$$\partial_z\mathcal{A} + k_1\partial_t\mathcal{A} = T + i\sum_{m=2}^{\infty}k_m\frac{(i\partial_t)^2}{m!}\mathcal{A}. \tag{8}$$

This chief equation is derived in Supplement 1. In the special case of continuous-wave (cw) operation, (8) reduces to the equation reported in [29]. The term T accounts for the nonlinear interaction and is defined as:

$$T \equiv \frac{ie^{-i\varphi}}{4\omega N} \int_{-\infty}^{\infty} \Omega^2 e^{-i\Omega t} \iint_{\mathbb{R}^2} \left[\vec{\tilde{\mathcal{P}}}^{(\mathrm{NL})}(\Omega) \cdot \vec{\mathfrak{e}}^* \, \mathrm{d}x \, \mathrm{d}y \right] \mathrm{d}\Omega \,, \tag{9}$$

where $\vec{\tilde{\mathcal{P}}}^{(\mathrm{NL})}$ is the Fourier component of the nonlinear polarization and depends on the nonlinear effect of interest.

Degenerate four-wave mixing is now considered, for which:

$$\vec{\tilde{\mathcal{P}}}^{(3)}(\Omega) = 3\varepsilon_0 \delta(\Omega - \omega) e^{-\alpha z} e^{ikz} \mathcal{A} \left| \mathcal{A} \right|^2 C\vec{v}, \tag{10}$$

where ε_0 is the vacuum permittivity, C is the third-order nonlinear tensor that has been reduced by assuming Kleinmann symmetry [30] and $\vec{v}$ is a complex 10-row vector that involves the components of the electric mode profile. These quantities are used in the definition of a unitless coupling coefficient:

$$\kappa \equiv \frac{c\varepsilon_0}{4N} \iint_{\mathbb{R}^2} (C\vec{v}) \cdot \vec{\mathfrak{e}}^* \, \mathrm{d}x \, \mathrm{d}y \,. \tag{11}$$

For amorphous materials, the C tensor contains only one independent coefficient (c_{11}), and [31]:

$$(C\vec{v}) \cdot \vec{\mathfrak{e}}^* = \frac{c_{11}}{3} \left[\left(\vec{\mathfrak{e}} \cdot \vec{\mathfrak{e}} \right)^2 + 2 \left(\vec{\mathfrak{e}} \cdot \vec{\mathfrak{e}}^* \right)^2 \right]. \tag{12}$$

Using (10) and (11) the term (9) simplifies to:

$$T = i\Gamma e^{-\alpha z} \mathcal{A} \left| \mathcal{A} \right|^2, \tag{13}$$

where:

$$\Gamma \equiv 3\frac{\omega}{c}\kappa. \tag{14}$$

Inserting (13) into (8):

$$\partial_z \mathcal{A} + k_1 \partial_t \mathcal{A} = i\Gamma e^{-\alpha z} \mathcal{A} \left| \mathcal{A} \right|^2 + i \sum_{m=2}^{\infty} k_m \frac{(i\partial_t)^m}{m!} \mathcal{A}. \tag{15}$$

Relation (15) is a more general version of the nonlinear Schrödinger equation [32] that rigorously includes loss and the vectorial nature of the modes. This contrasts with derivations found in textbooks [25] where the longitudinal component of the electric field is neglected, and where the system is assumed lossless.

2.1. Temporal solitons

In the case where $k_m = 0$ for $m > 2$, the following function is an exact solution to (15):

$$\mathcal{A}(z,t) = \mathcal{A}_0 e^{Gz} \Big/ \cosh\left(\tau/\tau_0 \right) , \tag{16}$$

with the retarded time $\tau \equiv t - k_1 z$, a complex amplitude $\mathcal{A}_0$, a characteristic time τ_0 and a complex phase G. These parameters must satisfy the following conditions:

$$\left| \mathcal{A}_0 \right|^2 = -\frac{k_2}{\Gamma \tau_0^2}, \tag{17}$$

and:

$$G = -i\frac{k_2}{2\tau_0^2}. \tag{18}$$

A pulse given by (16) does not vary in shape. This is known as a temporal soliton [33–35].

The group velocity is defined as the speed of a pulse envelope. From (16) and the definition of τ, it is clear that k_1 is related to the group velocity v_g by:

$$k_1 = 1/v_g. \tag{19}$$

From (7), k_2 relates to the group-velocity dispersion (GVD). Equation (17) imposes that the sign of k_2 should be opposite to the sign of κ (seen from (14)). For bright solitons, a negative k_2 results in anomalous dispersion, and a positive κ [36]. If there is zero attenuation, these conditions also imply that τ_0 is real. Hence, τ_0 represents the temporal width of the pulse.

2.2. Group index

From (7) and (19), the group index can be found from:

$$n_g \equiv c/v_g = c\left.\frac{\mathrm{d}K}{\mathrm{d}\Omega}\right|_{\omega}. \tag{20}$$

This expression seems to be more general than the common expression [37]:

$$\bar{n}_g = n + \omega\frac{\mathrm{d}n}{\mathrm{d}\omega}. \tag{21}$$

Both expressions (20) and (21) are compared in Fig. 1 by plotting the error:

$$\epsilon \equiv (\bar{n}_g - n_g)/\bar{n}_g\,. \tag{22}$$

n_g and $\bar{n}_g$ are found from simulations of waveguides made from Si_3N_4 and GaAs. Both structures are enclosed in SiO_2 cladding. As the waveguide thickness increases, the mode confinement increases, converging towards a homogeneous waveguide. The simulations are made with a 2 µm wide waveguide with a varying thickness (the Si_3N_4 waveguide is not simulated with a thickness below 100 nm, as the mode becomes highly unconfined). Values found from (21) are in general higher with a finite difference found in the third digit, showing an excellent match between the two expressions. The common expression (21) has been found to match well experimentally [38], giving us confidence in the validity of the presented formalism.

3. Optical Kerr effect

An important implication of the NLS equAn important implication of the NLS equation is the optical Kerr effect. Under continuous-wave (cw) excitation, the NLS equation (15) reduces to:

$$\partial_z\mathcal{A} = i\Gamma e^{-\alpha z}\mathcal{A}\,|\mathcal{A}|^2\,. \tag{23}$$

The $\mathcal{A}$ function can be expressed as:

$$\mathcal{A} = e^{i\phi}A, \tag{24}$$

with a phase ϕ and a norm A, such that:

$$\partial_z\mathcal{A} = e^{i\phi}(\partial_z A + iA\partial_z\phi). \tag{25}$$

From (23) one deduces that $\partial_z A = 0$. Using the expression for the optical power:

$$P = Ne^{-\alpha z}A^2, \tag{26}$$

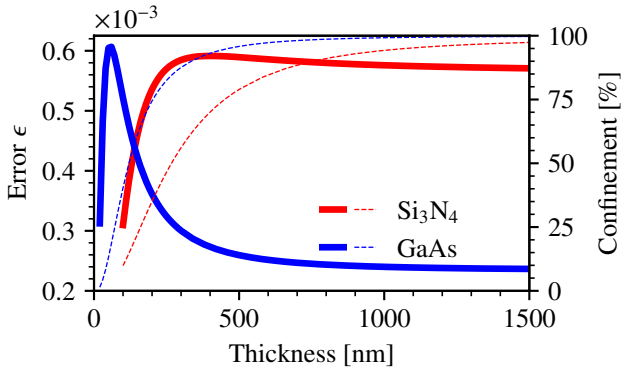

Fig. 1. Error (22) between the general expression (20) and the common expression (21) for the group index. Simulations are performed for a Si_3N_4 waveguide (in red) and a GaAs waveguide (in blue) as a function of the core thickness. Dashed lines show the confinement factor.

one finds:

$$\partial_z \phi = \frac{\Gamma}{N} P, \tag{27}$$

with Γ from (14). The third-order nonlinearity induces a phase change. This is known as the optical Kerr effect. One further defines a change of effective index by:

$$\Delta n \equiv \frac{c}{\omega} \partial_z \phi = n_2 P, \tag{28}$$

with the Kerr coefficient:

$$n_2 \equiv 3\kappa / N \ . \tag{29}$$

Notice that (28) is proportional to the power. This contrasts with the classical result from bulk optics where the optical Kerr effect induces a change of material refractive index proportional to the intensity.

For a waveguide based on amorphous materials, (12) applies. For waveguides with a negligible nonlinear contribution from the cladding, the coupling coefficient (11) reduces to:

$$\kappa = \frac{c\varepsilon_0}{12N} c_{11} \Sigma, \tag{30}$$

where:

$$\Sigma \equiv \iint_{\mathbb{R}^2} \left(\vec{\mathfrak{e}} \cdot \vec{\mathfrak{e}}\right)^2 + 2 \left(\vec{\mathfrak{e}} \cdot \vec{\mathfrak{e}}^*\right)^2 \mathrm{d}x \, \mathrm{d}y \ . \tag{31}$$

The Kerr coefficient can then be expressed as:

$$n_2 = \frac{c\varepsilon_0}{4N^2} c_{11} \Sigma. \tag{32}$$

Using the mode profile to calculate a nonlinear effective refractive index has been already reported, *e.g.* in Ref. [39]. The present formalism expands on this. Derived directly from the NLS equation, (29) is more general and works for all material systems.

Table 1. c_{11} Calculation.

$10^{-19}\,\bar{n}_2$ [m^2/W]	Si_3N_4 dim. ($w \times h$) [nm]	λ [nm]	A_{eff} [μm^2]	$10^{-7}\,n_2$ [W^{-1}]	$10^{-21}\,c_{11}$ [m^2/V^2]	Deposition method
3.12 ± 0.5 [42]	1650×700	1563	0.896	3.482	1.133 ± 0.8	LPCVD
2.4 [41]	1000×500	1550	0.802	2.994	0.655	PECVD
2.61 [43]	1600×660	1550	0.974	2.680	0.760	LPCVD

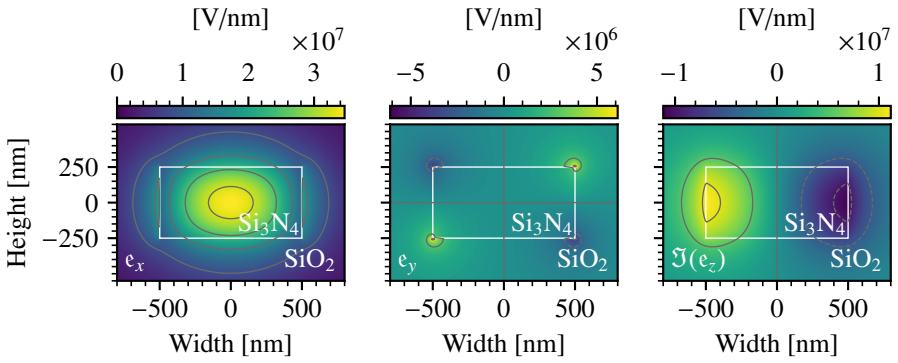

Fig. 2. Fundamental TE mode simulated at 1550 nm for a Si_3N_4 waveguide embedded in SiO_2. The waveguide core is 1000 nm wide and 500 nm thick, replicating the structure from [41]. A clear non-zero z component is visualized, motivating the derivation of the NLS equation without assuming this to be 0. The contour lines indicate a drop of 25%.

3.1. *Third-order nonlinear coefficient*

The usual formalism of the Kerr effect uses an effective area A_{eff} of the mode profile to have it represented with respect to intensity [40]. To translate it to the presented formalism, the Kerr coefficient $\bar{n}_2$, given in the intensity formalism, can be divided by the effective area A_{eff}.

This approach is used to find the c_{11} tensor element of amorphous Si_3N_4 from multiple previous works by using the measured Kerr coefficient reported in the intensity formalism in Si_3N_4 waveguides, see Table 1. Si_3N_4 is chosen as it has a high third-order nonlinearity [41], a broad transparency range [42], and is an amorphous material for which (32) is applicable. The waveguide structures in the investigated works are either a Si_3N_4 waveguide embedded by SiO_2 cladding [41, 42] or a substrate of SiO_2 with a Si_3N_4 waveguide embedded and air on top [43].

From these heterogeneous structures, the transverse integral in (11) is split into two parts, one for the cladding and one for the waveguide. The total effective Kerr coefficient is a sum of the effective Kerr coefficient stemming from both the waveguide core and the cladding:

$$n_2 = \frac{3c\varepsilon_0}{4N^2}\left(\Sigma_{\text{wg}} + \Sigma_{\text{clad}}\right), \tag{33}$$

with:

$$\Sigma_{\text{wg}} \equiv \iint_{\text{wg}} \left(C_{\text{wg}}\vec{v}\right) \cdot \vec{\mathfrak{e}}^{*}\, \mathrm{d}x\, \mathrm{d}y\,, \tag{34a}$$

and:

$$\Sigma_{\text{clad}} \equiv \iint_{\text{clad}} \left(C_{\text{clad}}\vec{v}\right) \cdot \vec{\mathfrak{e}}^{*}\, \mathrm{d}x\, \mathrm{d}y\,. \tag{34b}$$

The electric mode profiles $\vec{\mathbf{e}}$ are obtained from mode simulation, leaving the c_{11} tensor element for each material as the unknown variables. Using existing values of c_{11} for SiO_2 of $0.389 \times 10^{-22}\,\mathrm{m}^2/\mathrm{V}^2$ [44], c_{11} for Si_3N_4 can be found.

In literature sources where the effective area is not provided [41,42], it is instead found from mode simulations using the provided waveguide geometries in EMode [45]. All three papers considered the fundamental TE mode. The simulated mode profiles have waveguide confinement of 70-90%, with an evanescent field extending into the cladding. As an example, the mode profile of the waveguide from [41] is plotted in Figure 2. With low waveguide confinement, using a model that allows for heterogeneous structures becomes necessary.

The c_{11} coefficient found from each literature source results in a value for Si_3N_4:

$$c_{11} = 0.849 \times 10^{-21}\,\mathrm{m}^2/\mathrm{V}^2. \tag{35}$$

Not all sources provided uncertainties for their measurements, preventing error estimation. The variations in values can be a result of the manufacturing process, as the flow ratio during chemical vapor deposition (CVD) has been shown to modify the stoichiometry of SiN films [46,47]. The high uncertainty on the measurements from [42], and the resulting high uncertainties found for the nonlinear tensor elements, are also seen in other materials, such as barium borate (BBO) [48].

4. Discussion

The presented NLS equation for integrated photonics differs from the currently accepted derivations in multiple aspects. In particular, it avoids a series of assumptions such as plane wave propagation, the magnitude of the longitudinal component along $\hat{z}$, the existence of the optical Kerr effect, and the magnitude of the nonlinear effects. Lastly, the derivation is conducted using the complex wavenumber $\vec{k}$, which includes a finite value of attenuation through the entire derivation. By including the attenuation through the entire derivation, the resulting chief equation and NLS equation give insight into how attenuation affects nonlinear mode coupling. Nonlinear effects such as two-photon absorption, stimulated Raman scattering, and stimulated Brillouin scattering are not explicitly included in the derivation on the NLS equation, but could, along with other nonlinear effects, be included in $\vec{\mathcal{P}}^{(\mathrm{NL})}$ in the chief equation, (8), or in the attenuation coefficient.

As the presented explicit formula for the group index, (20), shows good coincidence with the conventional expression, (21), our confidence in the validity of the presented formalism is very high. Having an explicit formula for the group index, and therefore GVD, provides more insights into how to engineer these quantities to desired values, *e.g.* normal or anomalous dispersion.

The optical Kerr effect given by optical power is optimal for higher-order modes, where the effective area is a bad representation of the intensity. Two different modes can exhibit the same effective area, but a non-fundamental mode can achieve a substantially higher peak intensity, increasing the Kerr effect. Power is also used more in a laboratory setting, and hence a more convenient quantity for calculations. As the model allows for heterogeneous waveguides, its strength is apparent when a significant part of the mode profile leaks into the cladding/substrate, as in thin waveguides, leading to multiple contributions to the generated phase shift. The contributions are accounted for in (11) by splitting the integral into as many terms as there are nonlinear contributions, as done in the presented example. Combined with the presented method for calculating c_{11}, the expression for the Kerr coefficient given in this paper will allow for better predictions in the design of devices utilizing the Kerr effect, such as all-optical switches. The limiting factor for the accuracy of the model now becomes the large uncertainties in the C tensor elements, especially for non-amorphous materials with multiple independent tensor elements [48,49].

5. Conclusion

This study introduces a novel formalism for describing nonlinear integrated photonics, derived from a generalized chief equation. The resulting nonlinear Schrödinger equation is applied to the case of degenerate four-wave mixing, revealing a bright soliton solution. The NLS equation is used to derive a more general formula for the group index, providing a more accurate representation of integrated photonics compared to conventional expressions. Moreover, the optical Kerr effect is expressed in terms of optical power, yielding a Kerr coefficient that depends explicitly on the waveguide mode and power. The application of this formalism is demonstrated by calculating the relevant nonlinear tensor coefficient for Si_3N_4. This study enhances understanding of nonlinear effects in waveguides and offers practical tools for optical engineers in predicting nonlinear effects, especially nonlinear phase shifts.

Funding

We acknowledge support from Innovation Fund Denmark (Grand Solutions, FireQ project).

Disclosures

The authors declare no conflicts of interest.

Data avaibility

Data underlying the results presented in this paper are not publicly available at this time but may be obtained from the authors upon reasonable request.

Supplementary material

See Supplement 1 for supporting content.

References

1. Y. Kodama and A. Hasegawa, "Nonlinear pulse propagation in a monomode dielectric guide," IEEE J. Quantum Electron. **23**, 510–524 (1987).
2. B. Corcoran, M. Tan, X. Xu, A. Boes, J. Wu, T. G. Nguyen, S. T. Chu, B. E. Little, R. Morandotti, A. Mitchell, and D. J. Moss, "Ultra-dense optical data transmission over standard fibre with a single chip source," Nat. Commun. **11**, 2568 (2020).
3. H. Leopardi, J. Davila-Rodriguez, F. Quinlan, J. Olson, J. A. Sherman, S. A. Diddams, and T. M. Fortier, "Single-branch Er:fiber frequency comb for precision optical metrology with 10^{-18} fractional instability," Optica **4**, 879–885 (2017).
4. A. Schliesser, N. Picqué, and T. W. Hänsch, "Mid-infrared frequency combs," Nat. Photonics **6**, 440–449 (2012).
5. S. Ghanbari, R. Akbari, and A. Major, "Femtosecond Kerr-lens mode-locked alexandrite laser," Opt. Express **24**, 14836–14840 (2016).
6. F.-F. Du, G. Fan, X.-M. Ren, and M. Ma, "Deterministic hyperparallel control gates with weak Kerr effects," Adv. Quantum Technol. **6**, 2300201 (2023).
7. Y. Wang, C. F. Faurby, F. Ruf, P. I. Sund, K. Nielsen, N. Volet, M. J. Heck, N. Bart, A. D. Wieck, A. Ludwig *et al.*, "Deterministic photon source interfaced with a programmable silicon-nitride integrated circuit," NPJ Quantum Inf. **9**, 94 (2023).
8. X. Xue and N. Calabretta, "Nanosecond optical switching and control system for data center networks," Nat. Commun. **13**, 2257 (2022).
9. F. Ruf, L. Nielsen, N. Volet, and M. J. Heck, "Analysis and design of low-loss and fast all-optical switch elements on silicon nitride for integrated quantum photonics," J. Light. Technol. **40**, 7598–7609 (2022).
10. E. Lucas, S.-P. Yu, T. C. Briles, D. R. Carlson, and S. B. Papp, "Tailoring microcombs with inverse-designed, meta-dispersion microresonators," Nat. Photonics **17**, 943–950 (2023).
11. E. F. Perez, G. Moille, X. Lu, J. Stone, F. Zhou, and K. Srinivasan, "High-performance Kerr microresonator optical parametric oscillator on a silicon chip," Nat. Commun. **14**, 242 (2023).
12. D. T. Spencer, T. Drake, T. C. Briles, J. Stone, L. C. Sinclair, C. Fredrick, Q. Li, D. Westly, B. R. Ilic, A. Bluestone, N. Volet, T. Komljenovic, L. Chang, S. H. Lee, D. Y. Oh, M.-G. Suh, K. Y. Yang, M. H. P. Pfeiffer, T. J. Kippenberg, E. Norberg, L. Theogarajan, K. Vahala, N. R. Newbury, K. Srinivasan, J. E. Bowers, S. A. Diddams, and S. B. Papp, "An optical-frequency synthesizer using integrated photonics," Nature **557**, 81–85 (2018).
13. H. Bergeron, L. C. Sinclair, W. C. Swann, C. W. Nelson, J.-D. Deschênes, E. Baumann, F. R. Giorgetta, I. Coddington, and N. R. Newbury, "Tight real-time synchronization of a microwave clock to an optical clock across a turbulent air path," Optica **3**, 441–447 (2016).
14. E. Z. Ulsig, I. Degli-Eredi, E. J. Stanton, and N. Volet, "Efficient low threshold frequency conversion in AlGaAs-on-insulator waveguides," Front. Photon. **3**, 904651 (2022).
15. E. J. Stanton, P. Tønning, E. Z. Ulsig, S. Calmar, M. A. Bourland, S. T. Thomsen, K. B. Gravesen, P. Johansen, and N. Volet, "Continuous-wave second-harmonic generation in the far-uvc pumped by a blue laser diode," arXiv, 2309.04554 (2023).
16. J. M. Dudley, G. Genty, and S. Coen, "Supercontinuum generation in photonic crystal fiber," Rev. Mod. Phys. **78**, 1135 (2006).
17. V. N. Serkin and A. Hasegawa, "Novel soliton solutions of the nonlinear Schrödinger equation model," Phys. Rev. Lett. **85**, 4502 (2000).
18. Y. Shen, *The Principles of Nonlinear Optics* (Wiley, 1984).
19. R. W. Boyd, *Nonlinear Optics* (Academic Press, 2020).
20. P. S. Kuo and M. Fejer, "Mixing of polarization states in zincblende nonlinear optical crystals," Opt. Express **26**, 26971–26984 (2018).
21. T. J. Kippenberg, A. L. Gaeta, M. Lipson, and M. L. Gorodetsky, "Dissipative Kerr solitons in optical microresonators," Science **361**, eaan8083 (2018).
22. A. Boes, B. Corcoran, L. Chang, J. Bowers, and A. Mitchell, "Status and potential of lithium niobate on insulator (LNOI) for photonic integrated circuits," Laser Photonics Rev. **12**, 1700256 (2018).
23. G. Poberaj, H. Hu, W. Sohler, and P. Günter, "Lithium niobate on insulator (LNOI) for micro-photonic devices," Laser Photonics Rev. **6**, 488–503 (2012).
24. X. Han, M. Yuan, H. Xiao, G. Ren, T. G. Nguyen, A. Boes, Y. Su, A. Mitchell, and Y. Tian, "Integrated photonics on the dielectrically loaded lithium niobate on insulator platform," J. Opt. Soc. Am. B **40**, D26–D37 (2023).
25. G. P. Agrawal, *Nonlinear fiber optics* (Springer, 2019), 6th ed.
26. M. L. Madsen, E. Z. Ulsig, S. Folsach, P. H. Godoy, E. J. Stanton, and N. Volet, "Mid-infrared difference-frequency generation in AlGaAs-on-insulator waveguides," J. Opt. Soc. Am. B **40**, 1742–1748 (2023).
27. M. T. Hansen, E. Z. Ulsig, F. Labbé, M. L. Madsen, Y. Ding, K. Rottwitt, and N. Volet, "Efficient and robust second-harmonic generation in thin-film lithium niobate using modal phase matching," Front. Photon. **4**, 1324648 (2023).
28. Z. Zhu and T. G. Brown, "Full-vectorial finite-difference analysis of microstructured optical fibers," Opt. Express **10**, 853–864 (2002).
29. G. I. Stegeman and C. T. Seaton, "Nonlinear integrated optics," J. Appl. Phys. **58**, R57–R78 (1985).
30. X.-l. Yang and S.-w. Xie, "Expression of third-order effective nonlinear susceptibility for third-harmonic generation

in crystals," Appl. Opt. **34**, 6130–6135 (1995).
31. P. S. Banks, M. D. Feit, and M. D. Perry, "High-intensity third-harmonic generation," J. Opt. Soc. Am. B **19**, 102–118 (2002).
32. A. Hasegawa and F. Tappert, "Transmission of stationary nonlinear optical pulses in dispersive dielectric fibers. i. anomalous dispersion," Appl. Phys. Lett. **23**, 142–144 (1973).
33. M. Nakazawa, "Soliton transmission in telecommunication networks," IEEE Commun. Mag. **32**, 34–41 (1994).
34. T. Herr, V. Brasch, J. D. Jost, C. Y. Wang, N. M. Kondratiev, M. L. Gorodetsky, and T. J. Kippenberg, "Temporal solitons in optical microresonators," Nat. Photonics **8**, 145–152 (2014).
35. A. Jørgensen, D. Kong, M. Henriksen, F. Klejs, Z. Ye, Ò. Helgason, H. Hansen, H. Hu, M. Yankov, S. Forchhammer *et al.*, "Petabit-per-second data transmission using a chip-scale microcomb ring resonator source," Nat. Photonics **16**, 798–802 (2022).
36. Y. S. Kivshar and B. Luther-Davies, "Dark optical solitons: physics and applications," Phys. Rep. **298**, 81–197 (1998).
37. H. Danielmeyer and H. Weber, "Direct measurement of the group velocity of light," Phys. Rev. A **3**, 1708 (1971).
38. C. A. Barrios, B. Sánchez, K. B. Gylfason, A. Griol, H. Sohlström, M. Holgado, and R. Casquel, "Demonstration of slot-waveguide structures on silicon nitride/silicon oxide platform," Opt. Express **15**, 6846–6856 (2007).
39. B. Zabelich, E. Nitiss, A. Stroganov, and C.-S. Bres, "Linear electro-optic effect in silicon nitride waveguides enabled by electric-field poling," ACS Photonics **9**, 3374–3383 (2022).
40. Q. Lin, O. J. Painter, and G. P. Agrawal, "Nonlinear optical phenomena in silicon waveguides: modeling and applications," Opt. Express **15**, 16604–16644 (2007).
41. K. Ikeda, R. E. Saperstein, N. Alic, and Y. Fainman, "Thermal and Kerr nonlinear properties of plasma-deposited silicon nitride/silicon dioxide waveguides," Opt. Express **16**, 12987–12994 (2008).
42. C. J. Krückel, A. Fülöp, Z. Ye, P. A. Andrekson *et al.*, "Optical bandgap engineering in nonlinear silicon nitride waveguides," Opt. Express **25**, 15370–15380 (2017).
43. Y. Qu, J. Wu, Y. Yang, Y. Zhang, Y. Liang, H. El Dirani, R. Crochemore, P. Demongodin, C. Sciancalepore, C. Grillet *et al.*, "Enhanced four-wave mixing in silicon nitride waveguides integrated with 2D layered graphene oxide films," Adv. Opt. Mater. **8**, 2001048 (2020).
44. B. Buchalter and G. R. Meredith, "Third-order optical susceptibility of glasses determined by third harmonic generation," Appl. Opt. **21**, 3221–3224 (1982).
45. EMode (version 0.0.6-b4) [Software] from EMode Photonix. Available at emodephotonix.com.
46. C. J. Krückel, A. Fülöp, T. Klintberg, J. Bengtsson, P. A. Andrekson *et al.*, "Linear and nonlinear characterization of low-stress high-confinement silicon-rich nitride waveguides," Opt. Express **23**, 25827–25837 (2015).
47. T. Wang, D. K. Ng, S.-K. Ng, Y.-T. Toh, A. K. Chee, G. F. Chen, Q. Wang, and D. T. Tan, "Supercontinuum generation in bandgap engineered, back-end CMOS compatible silicon rich nitride waveguides," Laser Photonics Rev. **9**, 498–506 (2015).
48. M. Bache, H. Guo, B. Zhou, and X. Zeng, "The anisotropic Kerr nonlinear refractive index of the beta-barium borate (β-BaB_2O_4) nonlinear crystal," Opt. Mater. Express **3**, 357–382 (2013).
49. E. Dremetsika, B. Dlubak, S.-P. Gorza, C. Ciret, M.-B. Martin, S. Hofmann, P. Seneor, D. Dolfi, S. Massar, P. Emplit *et al.*, "Measuring the nonlinear refractive index of graphene using the optical Kerr effect method," Opt. Lett. **41**, 3281–3284 (2016).